JOURNAL OF GUIDANCE, CONTROL, AND DYNAMICS
Vol. 20, No. 2, March–April 1997

Slewing Flexible Spacecraft with Deflection-Limiting Input Shaping

William E. Singhose*
Massachusetts Institute of Technology, Cambridge, Massachusetts 02139
Arun K. Banerjee†
Lockheed Palo Alto Research Laboratory, Palo Alto, California 94304
and
Warren P. Seering‡
Massachusetts Institute of Technology, Cambridge, Massachusetts 02139

A control scheme is described for slewing flexible spacecraft with both suppression of deflection during the slew and elimination of residual oscillations. The method minimizes the maneuver time subject to constraints on residual vibration magnitude, sensitivity to modeling errors, rest-to-rest slew distance, and the transient deflection amplitude. Furthermore, a solution is sought that provides inherent fuel efficiency. The feasibility of the approach is demonstrated with linear and nonlinear computer simulations.

I. Introduction

APPLICATIONS such as reorienting the Space Shuttle with a payload attached to the remote manipulator require large angle slewing with suppression of elastic modes. When the maneuver time is minimized without regard to system flexibility, large amplitude transient and steady-state oscillations may occur, especially when the system is equipped with on–off reaction jets. The objective in such applications is often a rest-to-rest slew with limited vibration both during and at the end of the maneuver. For example, it may be necessary to generate a torque profile such that a system like the one shown in Fig. 1a is rotated through a desired angle θ_1, while the deflection θ_2 remains small throughout the slew and goes to zero at the end of the slew. A similar problem would be to move the system shown in Fig. 1b a finite distance, while limiting the maximum spring compression and eliminating the residual vibration.

Considerable work has been done in recent years on the topic of slewing with vibration control. Closed-loop, near-minimum time control based on Liapunov and sliding-mode techniques has been presented.[1,2] Calculus of variations was used to generate command profiles designed to minimize vibration in a simple flexible spacecraft model.[3] Shaped torque commands constructed from finite trigonometric series were proposed for minimizing modal vibration in a flexible satellite system.[4] Profiles designed using optimal control techniques were applied to a model of a spacecraft with flexible appendages.[5] Time-optimal rest-to-rest slewing of flexible systems has been investigated by several authors.[6–11] The need to conserve jet fuel has motivated the study of fuel-optimal and fuel/time-optimal control.[12–15]

The robust method of input shaping[16] has been proposed as a control method for flexible spacecraft. Input shaping is implemented by convolving a sequence of impulses, an input shaper, with a desired system command to produce a shaped input that then is used to drive the system. This process is demonstrated in Fig. 2. The amplitudes and time locations of the impulses are determined by solving a set of constraint equations that attempt to control the dynamic response of the system.

If the constraint equations only require zero residual vibration, then the resulting shaper is called a zero vibration (ZV) shaper. A ZV shaper will not work well on many systems because it will be sensitive to modeling errors. The earliest incarnation of ZV shaping was the technique of posicast control developed in the 1950s.[17,18] For input shaping to work well on most real systems, the constraint equations must ensure robustness to modeling errors. Singer and Seering[16] developed a form of robust input shaping by setting the derivative with respect to the frequency of the residual vibration equal to zero. The resulting shaper is called a zero vibration and derivative (ZVD) shaper.

Flexible spacecraft equipped with on–off reaction jets cannot produce the variable-amplitude actuation force that is usually required with input shaping; the spacecraft must be moved with constant-amplitude force pulses. Some heuristic methods for extending input shaping to the case of on–off actuators have been developed.[19] Use of constraints on the impulse amplitudes have been used to generate

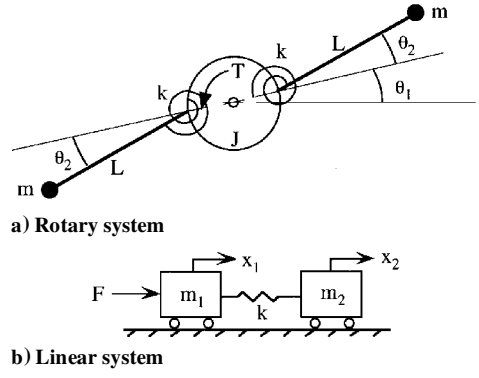

Fig. 1 Simple models used to formulate deflection-limiting input shaping.

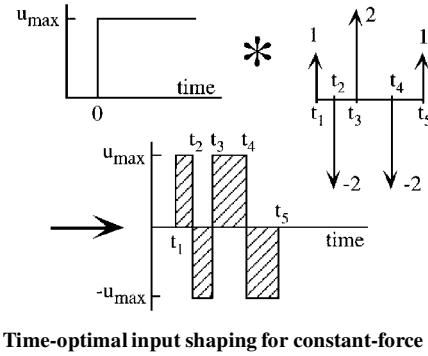

Fig. 2 Time-optimal input shaping for constant-force actuators.

Received March 1, 1996; revision received Sept. 23, 1996; accepted for publication Oct. 25, 1996.

*Research Assistant, Department of Mechanical Engineering. Member AIAA.
†Consulting Scientist, Dynamics and Control Laboratory.
‡Professor, Department of Mechanical Engineering.

time-optimal command profiles for on–off reaction jets. Liu and Wie,[7] Singh and Vadali,[9] and Wie et al.[20] demonstrated on–off input shaping with mass, spring, and damper simulations. Singhose et al.[10] used a detailed nonlinear simulation of the Space Shuttle's remote manipulator and hardware experiments to demonstrate extra-robust input shaping for on–off actuators. A recent extension to the preceding work has generated robust near time-optimal on–off control that is very fuel efficient.[21] A special case of on–off input shaping has been shown to be the time-optimal flexible-body control for a certain class of systems.[22]

The previous papers on input shaping for on–off control have concentrated on eliminating residual vibration. No constraints were placed on the amplitude of deflection during the slew. Input shaping is very successful at eliminating residual vibration and has the benefit of decreasing transient deflection when compared to bang-bang control.[23] However, the amplitude of the transient deflection is not limited and still can be very large. It is well known that large structural deflections induce large internal loads, and hence, deflection limiting is very important.

This paper presents a robust input shaping method for limiting deflection during the slew. This problem is significantly different from the earlier input shaping problem formulations. The difference arises from the nature of the constraint equations used to design the on–off control profiles. Previously, constraints were placed on the residual vibration amplitude, slew distance, etc., at a specific instant in time—the end of the command profile. However, limiting deflection during the slew requires constraints over the entire period of the slew.

Three procedures for obtaining deflection-limiting input shapers will be presented. The first method places constraints on the extrema points of the system's deflection. This method yields responses that precisely meet the desired deflection amplitude, but the solutions are difficult to obtain when the deflection is severely limited. The second method yields approximate solutions by limiting the deflection amplitude at specific time intervals rather than at the extrema points. The final method constrains the global maximum deflection by placing a simulation of the system being controlled inside an optimization loop. This method is more difficult to use but has the ability to deal directly with multimode and nonlinear systems. Results from computer simulations are used throughout the paper to illustrate key results.

II. Constraints Used for Deflection-Limiting Input Shaping

One of the great advantages of input shaping is that it requires only simple system models like the ones shown in Fig. 1. Simple models can be used because input shaping can be made robust to modeling errors. The robustness allows the command profiles developed for simple systems to work effectively on more complex systems.[10,24]

The amplitudes and time locations of the impulses in an input shaper are determined by satisfying a set of constraint equations while minimizing the maneuver duration. Except for the simplest cases, a nonlinear optimization is used to solve for the input shaper. The constraints for on–off shaping that have been previously utilized can be categorized as follows: residual vibration constraints, robustness constraints, requirement of time optimality, rigid-body constraints, constraints on the impulse amplitudes, and fuel-efficiency constraints. In this paper an additional type of constraint is used: deflection constraints.

A. Residual Vibration Constraints

The constraint on residual vibration amplitude can be expressed conveniently as the ratio of residual vibration amplitude with input shaping to that without shaping. If we assume the system is a second-order harmonic oscillator, or can be decomposed into a set of second-order systems, then the vibration ratio can be determined from the expression for residual vibration amplitude from an impulse.[25] The vibration resulting from an input shaper is the superposition of the vibration resulting from the individual impulses that compose the input shaper. The vibration amplitude from a shaper is divided by the vibration from a single unity-magnitude impulse to get a shaped vs unshaped residual vibration ratio V:

$$V = e^{-\zeta\omega t_n}\sqrt{\left[\sum_{i=1}^{n} A_i e^{\zeta\omega t_i}\cos\left(\omega\sqrt{1-\zeta^2}t_i\right)\right]^2 + \left[\sum_{i=1}^{n} A_i e^{\zeta\omega t_i}\sin\left(\omega\sqrt{1-\zeta^2}t_i\right)\right]^2} \tag{1}$$

where n is the number of impulses in the input shaper, A_i and t_i are the amplitudes and time locations of the impulses, ω is the system vibration frequency, and ζ is the damping ratio. When V is set equal to zero, Eq. (1) is referred to as the zero vibration (ZV) constraint.

B. Robustness Constraints

In addition to limiting residual vibration amplitude, most input shaping formulations require some amount of robustness to modeling errors. The earliest form of robust input shaping was achieved by setting the derivative with respect to the frequency of the residual vibration equal to zero.[16] That is,

$$0 = \frac{\mathrm{d}}{\mathrm{d}\omega}\left\{e^{-\zeta\omega t_n}\sqrt{\left[\sum_{i=1}^{n} A_i e^{\zeta\omega t_i}\cos\left(\omega\sqrt{1-\zeta^2}t_i\right)\right]^2 + \left[\sum_{i=1}^{n} A_i e^{\zeta\omega t_i}\sin\left(\omega\sqrt{1-\zeta^2}t_i\right)\right]^2}\right\} \tag{2}$$

Although more effective robustness constraints have been proposed,[10,26,27] the ZVD constraints given in Eqs. (1) and (2) are used in this paper. Use of the ZVD constraints is justified because they are somewhat easier to describe, and the focus of this paper is on the limitation of transient deflections, not residual oscillations. The alternative robustness constraints are completely compatible with the deflection-limiting methods described here.

C. Requirement of Time Optimality

Given the transcendental nature of the preceding equations, there will always be multiple solutions to the constraint equations. To make the solution time optimal subject to the residual vibration and robustness constraints, the shaper must be made as short as possible. Therefore, the time optimality constraint is

$$\min(t_n) \tag{3}$$

where t_n is the time of the final impulse.

D. Rigid-Body Constraints

To ensure that the system's mass center will move the desired amount, constraints must be placed on the rigid-body response. For example, the linearized equations of motion of the system shown in Fig. 1a are

$$\begin{bmatrix} J+2m(R+L)^2 & 2m(R+L)L \\ 2m(R+L)L & 2mL^2 \end{bmatrix}\begin{bmatrix} \ddot{\theta}_1 \\ \ddot{\theta}_2 \end{bmatrix} = \begin{bmatrix} T \\ -2k\theta_2 \end{bmatrix} \tag{4}$$

where J is the moment of inertia of the main body, m is the mass of the particles at the end of the rod of length L, R is the distance from the center of the main body to the attachment point of the rods, k is

the rotational spring constant, and T is the torque on the main body. For rest-to-rest slewing, the rigid-body constraints are

$$\dot{\theta}_1(t_n) = 0 \tag{5}$$

$$\theta_1(t_n) = \theta_{1f} \tag{6}$$

where θ_{1f} is the desired final slew angle. In a system such as that shown in Fig. 1b, equations analogous to Eqs. (5) and (6) are used to constrain the rigid-body motion. Equations (5) and (6) are used throughout the remainder of the paper to represent generalized rigid-body constraints valid for both rotary and linear systems.

E. Amplitude Constraints

The time-optimal control for rest-to-rest slewing of the systems shown in Fig. 1 subject to Eq. (1) and/or Eq. (2) has been shown to be a multiswitch bang-bang profile.[6–9,11,22] Therefore, the time-optimal input to the system under consideration must consist of alternating positive and negative constant-amplitude force pulses. A multiswitch bang-bang profile can be generated by convolving a step input with an input shaper of the form

$$\begin{bmatrix} A_i \\ t_i \end{bmatrix} = \begin{bmatrix} 1 & -2 & 2 & -2 & \cdots & -2 & 1 \\ 0 & t_2 & t_3 & t_4 & \cdots & t_{n-1} & t_n \end{bmatrix} \tag{7}$$

where n is odd. Figure 2 demonstrates that a step convolved with this type of an input shaper results in the desired form of command. The amplitude of the step input is equal to the maximum actuator effort, $u_{\max}$. Equation 7 leads to the following constraints on the impulse amplitudes:

$$\begin{aligned} A_i &= 1 \qquad && i = 1, n \\ A_i &= 2(-1)^{i-1} \qquad && i = 2, \ldots, n-1 \end{aligned} \tag{8}$$

The constraints given by Eqs. (3) and (8) are equivalent to requiring the time-optimal control, given actuator limitations.[22] The requirement of Eq. (3) alone is not sufficient because the impulse amplitudes will be driven toward positive and negative infinity by the time-optimality requirement.

F. Fuel Efficiency Constraints

Solution of Eqs. (1–3), (5), (6), and (8) with V set equal to zero will yield the time-optimal command signal subject to the ZVD constraints. However, the resulting multiswitch bang-bang profile uses a large quantity of fuel. It has been shown that relaxing the requirement of time optimality leads to profiles that are very nearly time optimal, yet use considerably less propellant.[12,21] One method of obtaining fuel-efficient profiles is to replace the preceding amplitude constraints. The fuel-efficient amplitude constraints force the profile to consist of a series of positive pulses followed by a series of negative pulses.[21] That is, one looks for an input shaper with the following set of impulse amplitudes:

$$\begin{bmatrix} A_i \\ t_i \end{bmatrix} = \begin{bmatrix} 1 & -1 & 1 & \cdots & -1 & -1 & 1 & \cdots & -1 & 1 \\ 0 & t_2 & t_3 & \cdots & t_{n/2} & t_{(n/2+1)} & t_{(n/2+2)} & \cdots & t_{n-1} & t_n \end{bmatrix} \tag{9}$$

where n is even. Figure 3 shows that a step input convolved with this type of shaper results in a series of positive pulses followed by a series of negative pulses. Requiring the profile to have this structure introduces periods of coasting, which leads to fuel savings. Profiles of this form are remarkable because they are approximately 1% longer than the time-optimal profiles, but they routinely decrease fuel consumption by 30%.[21] The fuel-efficient amplitude constraints can be written as

$$\begin{aligned} A_i &= (-1)^{i+1} \qquad && i = 1, \ldots, n/2 \\ A_i &= (-1)^{i} \qquad && i = n/2+1, \ldots, n \end{aligned} \tag{10}$$

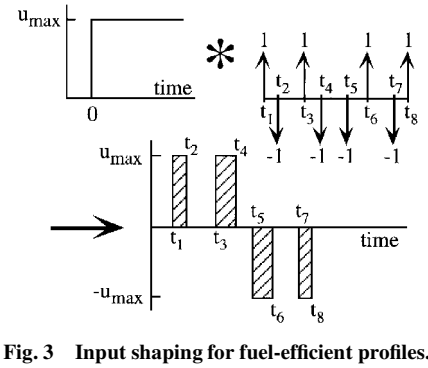

Fig. 3 Input shaping for fuel-efficient profiles.

G. Deflection Constraints

Solution of Eqs. (1–3), (5), (6), and (10) will lead to fuel-efficient commands that eliminate residual vibration and have some level of robustness to modeling errors. However, the deflection of the system during the slew is uncontrolled. If the deflection is large, the system may be damaged, or the endpoint may deviate considerably from an intended trajectory. To control the level of deflection during the slew, an expression for the deflection as a function of the input shaper must be obtained. The desired function can be generated using superposition of deflections from individual step inputs.

An expression for the deflection of the system shown in Fig. 1b is derived easily. The result is applicable to other systems with one flexible mode and a rigid-body mode, such as the system in Fig. 1a. The Laplace transforms of the equations of motion for the system shown in Fig. 1b are

$$\boldsymbol{F}(s) = \left(m_1 s^2 + k\right)\boldsymbol{x}_1(s) - k\boldsymbol{x}_2(s) \tag{11}$$

$$0 = \left(m_2 s^2 + k\right)\boldsymbol{x}_2(s) - k\boldsymbol{x}_1(s) \tag{12}$$

Equation (12) can be solved for $\boldsymbol{x}_2(s)$:

$$\boldsymbol{x}_2(s) = \frac{k}{\left(m_2 s^2 + k\right)}\boldsymbol{x}_1(s) \tag{13}$$

Combining Eqs. (11) and (13) and assuming $\boldsymbol{F}(s) = u_{\max}/s$ [assuming $F(t)$ is a step input of magnitude $u_{\max}$] gives

$$\boldsymbol{x}_1(s) = u_{\max}\left\{\frac{m_2 s^2 + k}{s^2[m_1 m_2 s^2 + (m_1 + m_2)k]}\right\} \tag{14}$$

The deflection for this system is the change in the natural length of the spring, which is defined as $D(t) = x_2(t) - x_1(t)$. Compression is a negative value; extension is positive. Therefore, from Eq. (13) we have

$$\boldsymbol{D}(s) = \left[\frac{k}{\left(m_2 s^2 + k\right)} - 1\right]\boldsymbol{x}_1(s) \tag{15}$$

substituting Eq. (14) into Eq. (15) yields

$$\boldsymbol{D}(s) = \frac{-u_{\max} m_2}{m_1 m_2}\left[\frac{1}{s(s^2 + \omega^2)}\right] \tag{16}$$

where

$$\omega^2 = \left(\frac{m_1 + m_2}{m_1 m_2}\right)k \tag{17}$$

Taking the inverse Laplace transform of Eq. (16), assuming zero initial conditions, gives the deflection from a step input as a function of time:

$$D(t) = (D_{\max}/2)[\cos(\omega t) - 1] \tag{18}$$

where ω is the natural frequency of oscillation and the maximum deflection magnitude $D_{\max}$ is given by

$$D_{\max} = \frac{2u_{\max} m_2}{k(m_1 + m_2)} \tag{19}$$

The coefficient in Eq. (18) is written as $D_{\max}/2$ because the quantity enclosed in the brackets has a maximum magnitude of two. A deflection equation with a structure identical to Eq. (18) can be derived similarly for the system shown in Fig. 1a.

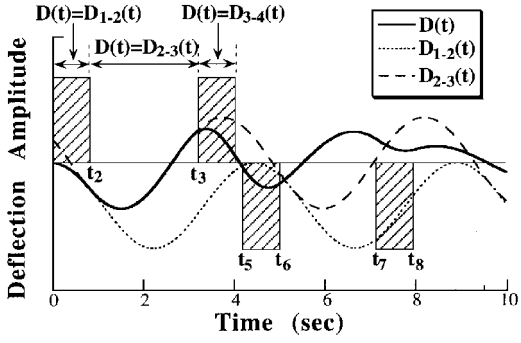

Fig. 4 Formation of the deflection function from piecewise-continuous segments.

Multiple versions of Eq. (18) can be used to generate a function that describes the deflection throughout a slew containing many step inputs (a pulse in force is composed of two step inputs—one positive and one negative delayed in time). Assuming that the command profile consists of a series of pulses obtained by using Eq. (10), then the deflection throughout the slew is given by

$$D(t) = D_{(m)-(m+1)}(t) \qquad t_m \le t < t_{m+1}, \quad m = 1, \ldots, n \quad (20)$$

where

$$D_{(m)-(m+1)}(t) = \sum_{i=1}^{m} A_i \frac{D_{\max}}{2}\{\cos[\omega(t - t_i)] - 1\} \quad (21)$$

Note the restriction presented by the qualifier $t_m \le t < t_{m+1}$. The deflection that occurs between the first and second impulses of the input, $D_{1-2}(t)$ (the period during the first pulse), is given by Eq. (20) when $m = 1$. The deflection $D_{2-3}(t)$ between the second and third impulses is given by Eq. (20) when $m = 2$. This is the coasting period between the first and second positive pulses (see Fig. 3). The deflection $D_{3-4}(t)$ that occurs during the second pulse is given by Eq. (20) with $m = 3$, etc. This process of generating the deflection function is illustrated in Fig. 4. Equation 20 amounts to a piecewise-continuous function composed of n finite-length segments; each of the segments has a limited range of applicability.

Note that the magnitude of deflection caused by a series of pulses can exceed $D_{\max}$ if the deflection components from individual pulses interfere constructively. The actual value of the parameter $D_{\max}$ is not needed if we generate the constraint equations in terms of a percentage deflection limit. We can form a nondimensional deflection limit D_L that is equal to the amplitude of the desired deflection, divided by $D_{\max}$. When the constraints are formed in this manner, the parameter $D_{\max}$ does not appear.

III. Limiting Local Extrema Points

One method to limit the maximum transient deflection is to locate all of the local extrema of the deflection function and place limits on the deflection amplitude at these instances. To obtain the extrema points of the deflection, Eq. (20) is differentiated with respect to time and the result is set equal to zero. The time values satisfying the resulting equation correspond to the extrema points. To obtain the general expression for the location of the extrema points, we first start with the extrema point that occurs between the first and second impulses. The deflection between impulses 1 and 2, $D_{1-2}(t)$, is obtained from Eq. (20) with $m = 1$:

$$D_{1-2}(t) = A_1(D_{\max}/2)[\cos(\omega t) - 1] \quad (22)$$

Differentiating Eq. (22) and setting the result to zero, we obtain

$$\frac{dD_{1-2}}{dt} = A_1 \frac{D_{\max}}{2}[-\omega \sin(\omega t)] = 0 \quad (23)$$

Equation (23) is satisfied by $\omega t = i\pi$, $i = 0, 1, 2, \ldots$. The even values of i correspond to times when the deflection is at a minimum (zero), whereas the odd values of i correspond to times when the magnitude of the deflection, $|x_2(t) - x_1(t)|$, is at a maximum—these are the times we are seeking. If we require that $D_{1-2}(t)$ given by Eq. (22) be less than a desired value at $t = \pi/\omega$, then we have obtained a deflection constraint equation that is a function of a specified time. The constraint can be written as

$$D_{1-2}(\pi/\omega) = A_1(D_{\max}/2)[\cos(\pi) - 1] = A_1 D_{\max} \le D_L \quad (24)$$

where D_L is the desired nondimensional deflection limit. Note that Eq. (24) is only an appropriate constraint if $t = \pi/\omega$ lies between the first and second impulses. If the second impulse occurs before $t = \pi/\omega$, then there will not be an extrema point of the deflection between the first and second impulse and, therefore, Eq. (24) is not a valid constraint.

The above process for obtaining deflection constraints can be repeated for all n segments of Eq. (20). The steps required for $m = 2$ are shown and then a general-purpose formula is given. When $m = 2$, the deflection between t_2 and t_3 is

$$D_{2-3}(t) = A_1(D_{\max}/2)[\cos(\omega t) - 1] + A_2(D_{\max}/2)\{\cos[\omega(t - t_2)] - 1\} \quad (25)$$

Differentiating Eq. (25), we obtain

$$\frac{dD_{2-3}}{dt} = A_1 \frac{D_{\max}}{2}[-\omega \sin(\omega t)] + A_2 \frac{D_{\max}}{2}\{-\omega \sin[\omega(t - t_2)]\} = 0 \quad (26)$$

Assuming that the impulse amplitudes are given by Eq. (10), then Eq. (26) is satisfied when

$$\sin(\omega t) = \sin[\omega(t - t_2)] \quad (27)$$

Expanding the term on the right-hand side yields

$$\sin(\omega t) = \sin(\omega t)\cos(\omega t_2) - \cos(\omega t)\sin(\omega t_2) \quad (28)$$

Dividing by $\cos(\omega t)$ and rearranging terms gives

$$\tan(\omega t) = \frac{-\sin(\omega t_2)}{1 - \cos(\omega t_2)} \quad (29)$$

Finally, taking the inverse tangent gives the extrema point between the second and third impulses:

$$t_{2-3} = \frac{1}{\omega}\tan^{-1}\left[\frac{-\sin(\omega t_2)}{1 - \cos(\omega t_2)}\right] \quad (30)$$

If t_{2-3} lies between the second and third impulses, then substituting t_{2-3} as given by Eq. (30) into Eq. (25) and limiting the resulting equation to below D_L is an appropriate constraint. Assuming that the impulse amplitudes are ± 1, the location of the extrema point between the impulses i and $(i + 1)$ is

$$t_{i-(i+1)} = \frac{1}{\omega}\tan^{-1}\left[\frac{\mathrm{sgn}(A_2)\sin(\omega t_2) + \mathrm{sgn}(A_3)\sin(\omega t_3) + \cdots + \mathrm{sgn}(A_i)\sin(\omega t_i)}{\mathrm{sgn}(A_1) + \mathrm{sgn}(A_2)\cos(\omega t_2) + \cdots + \mathrm{sgn}(A_i)\cos(\omega t_i)}\right] \quad (31)$$

where the signum function gives the sign of the impulse amplitude. The extrema points given by Eq. (31) are substituted back into the appropriate segment of Eq. (20) and the resulting equations are constrained to be below the desired deflection limit. If the deflection-constraint equations are solved simultaneously with the standard input-shaping constraint equations (1–3), (5), (6), and (10), then the resulting switch times will generate the deflection-limiting on–off command profile we are seeking.

To assess the above process, command profiles were designed for the system shown in Fig. 1b. A natural frequency of 0.2251 Hz was obtained by setting $m_1 = m_2 = k = u_{\max} = 1$. A desired move distance of 5 units was selected as a baseline case. A fuel-efficient

command profile was obtained by solving Eqs. (1–3), (5), (6), and (10); no deflection constraints were used. The required optimization was performed with the nonlinear optimization package GAMS.[28] The resulting fuel-efficient profile consists of two positive and two negative pulses described by

$$\begin{bmatrix} A_i \\ t_i \end{bmatrix} = \begin{bmatrix} 1 & -1 & 1 & -1 & -1 & 1 & -1 & 1 \\ 0 & 1.1998 & 2.3854 & 3.8605 & 3.8605 & 5.3356 & 6.5212 & 7.7210 \end{bmatrix} \tag{32}$$

The deflection resulting from the fuel-efficient profile is shown in Fig. 5. The maximum deflection is 0.75 units.

Deflection-limiting constraints were then added to the problem formulation, and a new optimization was performed, with the deflection limited to 0.6, so that the deflection would be 80% of the level with the unconstrained fuel-efficient profile. The 80% limited command profile consists of three positive and three negative pulses given by

$$\begin{bmatrix} A_i \\ t_i \end{bmatrix} = \begin{bmatrix} 1 & -1 & 1 & -1 & 1 & -1 & -1 & 1 & -1 & 1 & -1 & 1 \\ 0 & 0.9062 & 1.5359 & 2.0527 & 2.7770 & 3.9612 & 3.9612 & 5.1454 & 5.8698 & 6.3865 & 7.0162 & 7.9224 \end{bmatrix} \tag{33}$$

The response to the deflection-limiting profile is also shown in Fig. 5. Although the deflection is reduced 20%, the slew duration is increased only 2.6%. Note that the residual vibration is completely eliminated by both commands.

As a more rigorous test of this method, deflection-limiting command profiles were designed for the nonlinear Waves In Space Plasma (WISP) system.[24] The WISP system consists of two 150-m-long antenna booms attached to the Space Shuttle. A sketch of the system is shown in Fig. 6. When the system is moved using the shuttle thrusters, tens of meters of deflection can occur at the endpoints.

To apply the method, which is based on the simple models of Fig. 1, to the nonlinear WISP system, a simulation of the WISP system was performed using the nonlinear model previously described.[24] An approximate value for the fundamental period of 535 s was obtained from time response data and the damping was approximately zero. Using these two parameters and the actuator force-to-mass ratio, the WISP system was modeled as the system shown in Fig. 1a. A deflection-limiting input shaper was designed by limiting the extrema points as described above. The deflection limit was set so that the tip deflection would be 15 m. The resulting

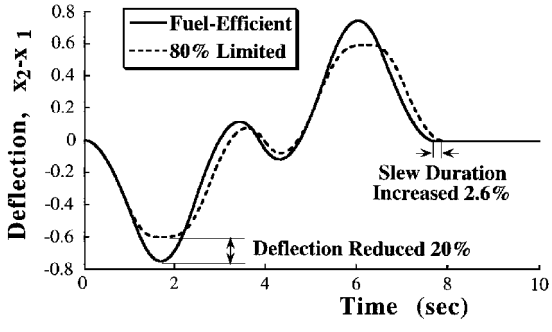

Fig. 5 Comparison of unrestricted and deflection-limited responses.

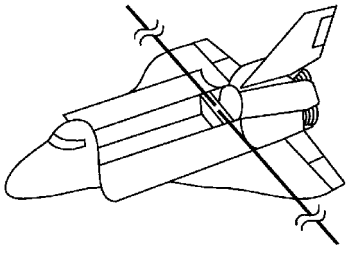

Fig. 6 WISP system.

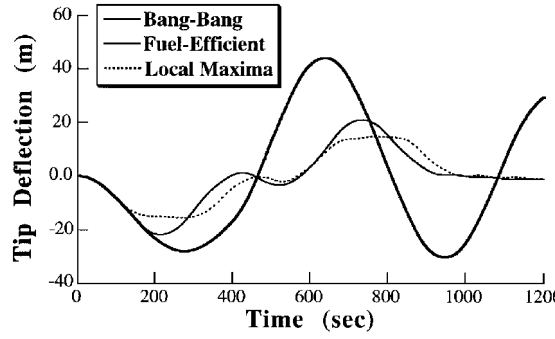

Fig. 7 Deflection responses of the WISP system.

command then was used as the input to the nonlinear WISP simulation. Figure 7 shows deflection responses to a bang-bang input, a fuel-efficient input, and the deflection-limited input. Not only is the residual oscillation virtually eliminated by the shaped profiles, but the deflection during the slew is very close to the design value. The profile designed for 15-m maximum deflection yields a tip deflection of 15.4 m. Although the profiles were designed using a simple, one-mode linear model, the robustness of the method provides excellent performance for the nonlinear system. The small level of residual vibration results from system nonlinearities and a second mode whose period is approximately 90 s.

Using the extrema points to limit the deflection becomes difficult when the deflection is severely limited. A problem arises because severe restrictions on the deflection amplitude require the use of numerous, short-duration pulses. Each additional pulse leads to two additional extrema points and consequently two additional versions of Eq. (31). Because the inverse tangent function is used in Eq. (31), a time value that falls within one period of the oscillation is returned. The time value must be shifted by an appropriate multiple of the half period to get the true time location of the extrema point. This time shifting becomes difficult to implement with large numbers of pulses and slews that take several vibration periods to complete.

IV. Deflection Sampling

In this section a procedure is presented that does not use Eq. (31); consequently, it can be used when large decreases in the deflection are desired. The method is an approximate method; however, it yields very good solutions. Rather than locate and limit the extrema points, the deflection given by Eq. (20) is constrained to be less than some tolerable percentage deflection D_L at periodic instances throughout the slew. That is, the deflection constraints are

$$D_L \geq \sum_{i=1}^{m} A_i \{\cos[\omega(t_s - t_i)] - 1\} \qquad t_m \leq t \leq t_{m+1} \qquad m = 1, \ldots, n \tag{34}$$

where t_s are specific instances in time at which the deflection function is sampled and required to be bounded by D_L. The process of deflection sampling is illustrated in Fig. 8. Note that this procedure does not guarantee that the deflection will be bounded by D_L at all times, only at the sampled times. However, by making the sampling points close together, the deflection can be effectively limited. The tradeoff is that as the accuracy of the solution is increased, the number of equations that must be satisfied increases.

Rather than using the fixed time interval sampling shown in Fig. 8, a fixed number of samples per force pulse and coast period is used. The primary reason for this choice is ease of implementation. During each pulse or coast period, the deflection constraint is given by one of the n equations listed in Eq. (34). By using R samples during each pulse or coast period, the constraints can be written easily as R versions of the n equations given in Eq. (34). That is, the deflection

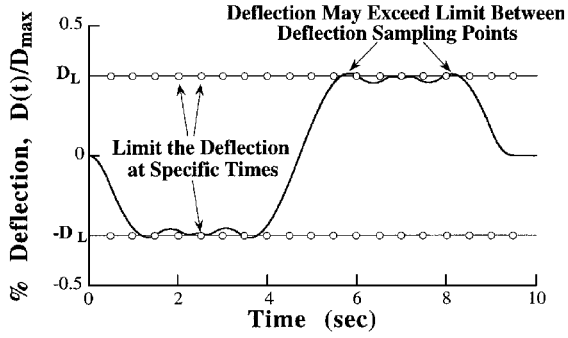

Fig. 8 Illustration of deflection sampling.

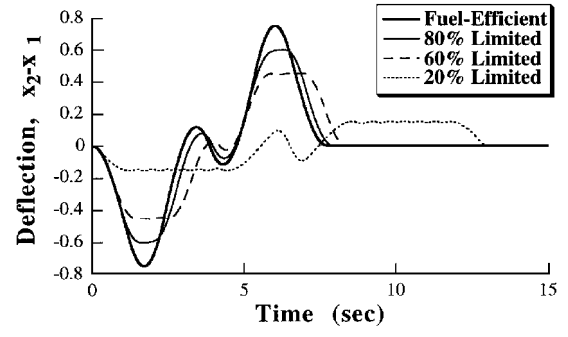

Fig. 9 Deflection curves of linear system for several values of the deflection limit.

constraints consist of R versions of Eq. (34) with $m = 1$, R versions of Eq. (34) with $m = 2$, etc. For a given value of m, the R equations differ in that the time locations, t_s, at which they are enforced is different. Within each pulse or coast period, the deflection is sampled at a resolution of $(t_{m+1} - t_m)/R$.

If a fixed-time-period sampling is used instead, the deflection constraint that must be used at each sampling point is then a function of the impulse times. Because the impulse times are being changed during the optimization and the change in impulse times triggers a change in the equations being optimized, the optimization becomes very difficult to perform.

To demonstrate the effectiveness of deflection sampling, new profiles were designed for the system of Fig. 1b using a sampling resolution of $R = 20$. The new profiles were designed to meet more severe deflection-limiting constraints. Figure 9 shows the responses of Fig. 5 along with responses when the deflection is limited to 60 and 20% of the baseline level. Note that in all cases the residual vibration is zero. Limiting the deflection causes the slew time to increase. The increase in slew time is small for the 80 and 60% limited profiles. The time penalty increases substantially as the deflection limit approaches zero. Even though deflection sampling is an approximate method, the deflection curves shown in Fig. 9 are all well within 1% of the desired deflection limit.

The effectiveness of deflection sampling depends on the sampling resolution. The appropriate choice of resolution depends on system parameters such as natural frequency and maneuver duration; however, the most important issue is the acceptable overshoot in maximum deflection amplitude. If the actual deflection is permitted to exceed D_L by a few percent, then the sampling resolution can be very coarse. Two or three samples per command pulse may be all that is needed. If, on the other hand, the deflection limit is a very strict design parameter, then the sampling resolution must be increased or the deflection limit must be decreased slightly to account for the overshoot between sampling points.

V. Using a Simulation Inside the Optimization Loop

The final method presented here for obtaining deflection-limiting shapers uses a numerical simulation within an optimization loop. To implement this scheme, the nonlinear constraint optimization software ADS[29] was used, choosing the option of modified method of feasible directions. The cost function minimized is the final time, Eq. (3), subject to Eqs. (1), (2), (5), (6), and (10). The deflection amplitude constraint is handled by numerically integrating the equations of motion up to the final time and noting the maximum tip deflection. This global maximum deflection is returned to the optimization and used to drive the search algorithm. All gradients needed in the optimization method are calculated by finite difference. Scaling of the robustness constraint (2) helps significantly in the convergence of the optimization process.

To proceed, one chooses a particular pulse profile [choose a specific value for n in Eq. (10)]. A solution is sought first, neglecting the deflection amplitude information provided by the simulation; this paves the way for "creeping up" on the solution. When the solution without deflection limiting is obtained, it is used as the initial guess for the optimization, which includes the simulation feedback. When the deflection limiting is first included in the constraints, D_L is initially set to a value very close to the deflection that occurs without any deflection constraints. When a solution is obtained, it is used as the initial guess for a more restrictive value of D_L. The process is repeated until the desired value of D_L is reached. The process is not a requirement; however, it facilitates the optimization.

Although this method usually requires the use of several optimizations, it can directly handle system nonlinearities if a nonlinear simulation is used for feedback to the optimization. Furthermore, it can easily accommodate multimode systems. To do this, one integrates the multimode system equations, analogous to Eq. (4), and constrains the global maximum deflection below the specified limit. To use the first two deflection-limiting methods on multimode systems requires the generation of a multimode deflection expression. That is, an expression analogous to Eq. (20) must be derived that accounts for the multiple modes.

VI. Comparison of Methods

Although the three methods described are significantly different in their approaches to the problem, they produce very similar command profiles. Limiting local extrema and using a simulation in the loop will produce exactly the same results if the system is perfectly linear. Deflection sampling will not produce exactly the same result because of its approximate nature.

When the system is nonlinear, each technique will produce a slightly different profile. When applied to the WISP system with a 15-m deflection limit, the techniques yield the following profiles:

Limiting local extrema:

$$\begin{bmatrix} A_i \\ t_i \end{bmatrix} = \begin{bmatrix} 1 & -1 & 1 & -1 & 1 & -2 & 1 & -1 & 1 & -1 & 1 \\ 0 & 97.6 & 180.1 & 284.2 & 372.1 & 495.2 & 618.3 & 706.1 & 810.3 & 892.7 & 990.3 \end{bmatrix} \tag{35}$$

Deflection sampling:

$$\begin{bmatrix} A_i \\ t_i \end{bmatrix} = \begin{bmatrix} 1 & -1 & 1 & -1 & 1 & -2 & 1 & -1 & 1 & -1 & 1 \\ 0 & 97.8 & 180.4 & 284.7 & 372.4 & 495.2 & 617.9 & 705.6 & 809.9 & 892.6 & 990.3 \end{bmatrix} \tag{36}$$

Simulation in the loop:

$$\begin{bmatrix} A_i \\ t_i \end{bmatrix} = \begin{bmatrix} 1 & -1 & 1 & -1 & 1 & -1 & -1 & 1 & -1 & 1 & -1 & 1 \\ 0 & 100.9 & 178.5 & 276.3 & 363.8 & 479.1 & 507.6 & 623.5 & 708.9 & 804.9 & 885.7 & 989.2 \end{bmatrix} \tag{37}$$

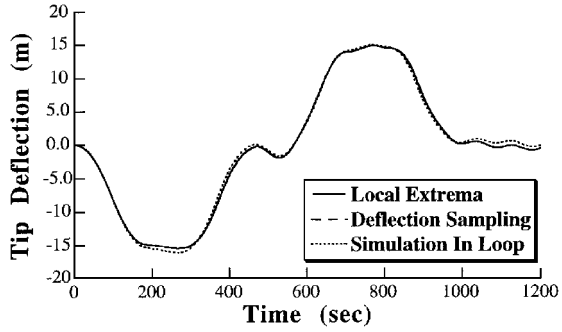

Fig. 10 Comparison of WISP response to three different profiles.

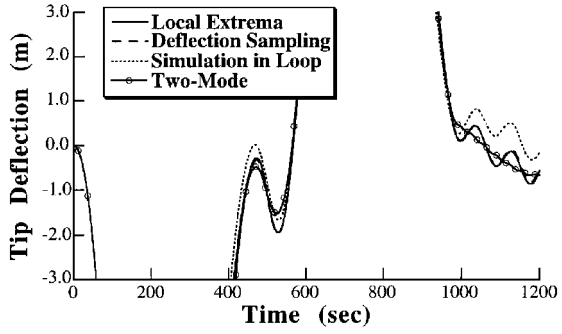

Fig. 11 WISP responses to single- and two-mode profiles.

The response to each of these profiles is shown in Fig. 10. All three methods limit the deflection to near the 15-m limit and produce very small levels of residual vibration.

VII. Multimode Systems

As mentioned previously, the small level of residual oscillation of the WISP system is composed partly of a secondary mode with a 90-s period. A command profile was generated using deflection sampling to eliminate this secondary mode by simply enforcing a second set of ZVD constraints at this higher mode. Figure 11 compares the response of this two-mode profile to the three responses shown in Fig. 10. The secondary mode has been completely eliminated. The downward trend in the response from 1000 to 1200 s is caused by the small-amplitude residual vibration of the low mode.

Note that the deflection of the second mode was not limited, only its residual amplitude. That is, the deflection constraints were based on the single-mode deflection expression given in Eq. (34). Multimode deflection constraints were not needed in this case because the first mode dominates the transient deflection amplitude. If a secondary mode contributes significantly to the deflection amplitude, then a two-mode deflection expression must be used with deflection sampling. The process of limiting the local extrema gets prohibitively complicated for multimode systems. Multimode system deflections are handled without added difficulty by the simulation-in-the-loop method.

VIII. Conclusions

Methods for limiting both transient and residual oscillations during the rest-to-rest slewing of flexible spacecraft have been presented. The techniques use a specialized form of input shaping to create appropriate on–off command profiles. Three procedures are presented for designing the necessary input shaper: 1) the extrema points of the deflection were located and limited, 2) the deflection was limited at discrete time locations, and 3) a simulation of the system was placed inside an optimization loop. Procedure 1 yields exact solutions but is difficult to implement when severe limitations are placed on the deflection or the system has multiple modes. Procedure 2 is the most straightforward and can be used effectively for cases of severe deflection limiting. Procedure 3 is both exact and direct but requires several optimizations.

The procedures were combined with previous input shaping techniques to obtain near time-optimal command profiles that robustly eliminate residual vibration and are very fuel-efficient. The deflection and residual oscillation reduction was demonstrated with computer simulations. Furthermore, the robustness of the technique was demonstrated with the use of nonlinear simulations.

Acknowledgment

Support for this work was provided by the Massachusetts Space Grant Fellowship Program.

References

[1]Byers, R. M., Vadali, S. R., and Junkins, J. L., "Near-Minimum Time, Closed-Loop Slewing of Flexible Spacecraft," *Journal of Guidance, Control, and Dynamics*, Vol. 13, No. 1, 1990, pp. 57–65.

[2]Junkins, J. L., Rahman, Z. H., and Bang, H., "Near-Minimum Time Control of Distributed Parameter Systems: Analytical and Experimental Results," *Journal of Guidance, Control, and Dynamics*, Vol. 14, No. 2, 1991, pp. 406–415.

[3]Farrenkopf, R. L., "Optimal Open-Loop Maneuver Profiles for Flexible Spacecraft," *Journal of Guidance and Control*, Vol. 2, No. 6, 1979, pp. 491–498.

[4]Swigert, C. J., "Shaped Torque Techniques," *Journal of Guidance and Control*, Vol. 3, No. 5, 1980, pp. 460–467.

[5]Turner, J. D., and Junkins, J. L., "Optimal Large-Angle Single-Axis Rotational Maneuvers of Flexible Spacecraft," *Journal of Guidance and Control*, Vol. 3, No. 6, 1980, pp. 578–585.

[6]Ben-Asher, J., Burns, J. A., and Cliff, E. M., "Time-Optimal Slewing of Flexible Spacecraft," *Journal of Guidance, Control, and Dynamics*, Vol. 15, No. 2, 1992, pp. 360–367.

[7]Liu, Q., and Wie, B., "Robust Time-Optimal Control of Uncertain Flexible Spacecraft," *Journal of Guidance, Control, and Dynamics*, Vol. 15, No. 3, 1992, pp. 597–604.

[8]Singh, G., Kabamba, P. T., and McClamroch, N. H., "Planar, Time-Optimal, Rest-to-Rest Slewing Maneuvers of Flexible Spacecraft," *Journal of Guidance, Control, and Dynamics*, Vol. 12, No. 1, 1989, pp. 71–81.

[9]Singh, T., and Vadali, S. R., "Robust Time-Optimal Control: A Frequency Domain Approach," *Journal of Guidance, Control, and Dynamics*, Vol. 17, No. 2, 1994, pp. 346–353.

[10]Singhose, W., Derezinski, S., and Singer, N., "Extra-Insensitive Input Shapers for Controlling Flexible Spacecraft," *Journal of Guidance, Control, and Dynamics*, Vol. 19, No. 2, 1996, pp. 385–391.

[11]Pao, L. Y., "Minimum-Time Control Characteristics of Flexible Structures," *Journal of Guidance, Control, and Dynamics*, Vol. 19, No. 1, 1996, pp. 123–129.

[12]Singh, T., "Fuel/Time Optimal Control of the Benchmark Problem," *Journal of Guidance, Control, and Dynamics*, Vol. 18, No. 6, 1995, pp. 1225–1231.

[13]Meyer, J. L., and Silverberg, L., "Fuel Optimal Propulsive Maneuver of an Experimental Structure Exhibiting Spacelike Dynamics," *Journal of Guidance, Control, and Dynamics*, Vol. 19, No. 1, 1996, pp. 141–149.

[14]VanderVelde, W., and He, J., "Design of Space Structure Control Systems Using On-Off Thrusters," *Journal of Guidance, Control, and Dynamics*, Vol. 6, No. 1, 1983, pp. 53–60.

[15]Wie, B., Sinha, R., Sunkel, J., and Cox, K., "Robust Fuel- and Time-Optimal Control of Uncertain Flexible Space Structures," *AIAA Guidance, Navigation, and Control Conference* (Monterey, CA), AIAA, Washington, DC, 1993, pp. 939–948 (AIAA Paper 93-3804).

[16]Singer, N. C., and Seering, W. P., "Preshaping Command Inputs to Reduce System Vibration," *Journal of Dynamic Systems, Measurement and Control*, Vol. 112, March 1990, pp. 76–82.

[17]Smith, O. J. M., "Posicast Control of Damped Oscillatory Systems," *Proceedings of the IRE*, Vol. 45, Sept. 1957, pp. 1249–1255.

[18]Smith, O. J. M., *Feedback Control Systems*, McGraw–Hill, New York, 1958, pp. 331–345.

[19]Rogers, K., and Seering, W. P., "Input Shaping for Limiting Loads and Vibration in Systems with On-Off Actuators," AIAA Guidance, Navigation, and Control Conf., San Diego, CA, 1996.

[20]Wie, B., Sinha, R., and Liu, Q., "Robust Time-Optimal Control of Uncertain Structural Dynamic Systems," *Journal of Guidance, Control, and Dynamics*, Vol. 15, No. 5, 1993, pp. 980–983.

[21]Singhose, W., Bohlke, K., and Seering, W., "Fuel-Efficient Pulse Command Profiles for Flexible Spacecraft," *Journal of Guidance, Control, and Dynamics*, Vol. 19, No. 4, 1996, pp. 954–960.

[22]Pao, L. Y., and Singhose, W. E., "On the Equivalence of Minimum Time Input Shaping with Traditional Time-Optimal Control," *IEEE Conference on Control Applications* (Albany, NY), Inst. of Electrical and Electronics Engineers, New York, 1995, pp. 1120–1125.

[23] Pao, L. Y., and Singhose, W. E., "A Comparison of Constant and Variable Amplitude Command Shaping Techniques for Vibration Reduction," *IEEE Conference on Control Applications* (Albany, NY), Inst. of Electrical and Electronics Engineers, New York, 1995, pp. 875–881.

[24] Banerjee, A. K., "Dynamics and Control of the WISP Shuttle-Antennae System," *Journal of Astronautical Sciences*, Vol. 41, No. 1, 1993, pp. 73–90.

[25] Bolz, R. E., and Tuve, G. L., *CRC Handbook of Tables for Applied Engineering Science*, CRC Press, Boca Raton, FL, 1973.

[26] Singhose, W., Seering, W., and Singer, N., "Residual Vibration Reduction Using Vector Diagrams to Generate Shaped Inputs," *Journal of Mechanical Design*, Vol. 116, June 1994, pp. 654–659.

[27] Singhose, W. E., Porter, L. J., Tuttle, T. D., and Singer, N. C., "Vibration Reduction Using Multi-Hump Input Shapers," *Journal of Dynamic Systems, Measurement and Control* (to be published).

[28] Brooke, A., Kendrick, D., and Meeraus, A., *GAMS: A User's Guide*, Scientific Press, Redwood City, CA, 1988.

[29] Vanderplaats, G. N., *ADS—A Fortran Program for Automated Design Synthesis, ver. 2.01, User's Manual*, Engineering Design Optimization, Inc., Santa Barbara, CA, 1987.